

COSMO-RS Analysis of CO₂ Solubility in *N*-Methyldiethanolamine, Sulfolane, and 1-Butyl-3-methyl-imidazolium Acetate Activated by 2-Methylpiperazine for Postcombustion Carbon Capture

Sweta Balchandani and Ramesh Singh*



Cite This: ACS Omega 2021, 6, 747–761



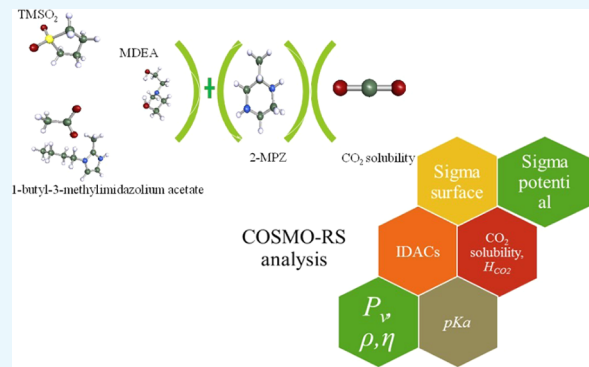
Read Online

ACCESS |

Metrics & More

Article Recommendations

ABSTRACT: Novel aqueous (aq) blends of *N*-methyldiethanolamine (MDEA), sulfolane (TMSO₂), and 1-butyl-3-methyl-imidazolium acetate ([bmim][Ac]) with amine activator 2-methylpiperazine (2-MPZ) are analyzed through conductor-like screening model for real solvents (COSMO-RS) for possible application in the chemisorption of CO₂. The molecules associated are analyzed for their ground-state energy, σ potential, and σ surface. Thermodynamic and physicochemical properties have been assessed and paralleled with the experimental data. Vapor pressure of the blended systems and pure component density and viscosity have been compared successfully with the experimental data. Important binary interaction parameters for the aqueous blends over a wide temperature, pressure, and concentration range have been estimated for NRTL, WILSON, and UNIQUAC 4 models. The COSMO-RS theory is further applied in calculating the expected CO₂ solubility over a pressure range of 1.0–3.0 bar and temperature range of 303.15–323.15 K. Henry's constant and free energy of solvation to realize the physical absorption through intermolecular interaction offered by the proposed solvents. Perceptive molecular learning from the behavior of chemical constituents involved indicated that the best suitable solvent is aq (MDEA + 2-MPZ).



1. INTRODUCTION

The quest to reduce CO₂ emissions via different routes has been a major concern over the past few decades. The process intensification of the existing CO₂ capture techniques and introduction of novel solvents for achieving the same through chemisorption or physisorption has been proposed by many researchers.^{1,2} An extensive lab-scale development of vapor–liquid equilibria,³ kinetic studies,⁴ thermophysical properties,^{5,6} calculation of binary interaction parameters,⁷ improvement in the existing modeling techniques,⁸ proposing new correlational analysis,⁹ optimizing the reaction or process parameters,¹⁰ defining the structural property relationships,¹¹ heat of absorption,¹² etc. are an integral part of the development of new solvents for CO₂ or other acid gas absorption applications. However, most of the experimental investigations at the pilot scale tend to be very expensive, and therefore, an efficient solvent screening through various analyses of the proposed solvents is the need of the hour to arrive at a conclusion of their possible applicability at the plant scale. Conclusively, researchers have shifted the research a step back at the quantum-molecular level to understand the basic phenomena of the novel solvents than to lab- or pilot-scale studies for achieving the anticipated CO₂ separation.^{13–17}

The conductor-like screening model for real solvents (COSMO-RS) is a method of quantum chemical calculations

grouped with statistical thermodynamics. The same has been widely applied for accurate prediction of thermodynamic or essential behavioral properties such as Gibb's free energy, activity coefficients, partition coefficients, etc. Calculating the highest occupied molecular orbital (HOMO) and lowest unoccupied molecular orbital (LUMO) gaps to define the polarities or electronegativities associated with a specific molecule yields a useful insight for behavioral analysis of any molecule.¹⁸ This significantly reduces the amount of time, energy, and cost associated with the detailed study required for a set of selected solvents. The variations of the predictive capabilities of COSMO-RS can be deduced from a brief literature survey. COSMO-RS applications in the membrane separation processes through COSMOic simulations have been widely studied in the recent past, indicating the efficiency of estimation of partition coefficients with fewer deviations from experimental studies in comparison to molecular dynamics simulation evaluations.^{19–23}

Received: October 30, 2020

Accepted: December 14, 2020

Published: December 30, 2020


Table 1. Specifications of the Chemicals Used in the Present Study

Chemical Name	Chemical Formula	Molecular weight	Source	Stated Mass fraction Purity	CAS no.	Purification method
1-butyl-3-methyl-imidazolium acetate ([bmim][Ac])	A chemical structure showing a cation part with a pyridine ring substituted at the 3-position with a methyl group and at the 1-position with a butyl chain, followed by an acetoxy group (-OCH ₃). The anion part is an acetate group (-OCH ₃).	198.26	Sigma-Aldrich Co.	≥0.95	284049-75-8	Vacuum drying for 48 hrs
<i>N</i> -Methyldiethanolamine (MDEA)	A chemical structure showing a tertiary amine with a methyl group on nitrogen and two ethyl groups attached to it, one of which is further substituted with a hydroxyl group.	119.16	Sigma-Aldrich Co.	≥0.99	105-59-9	None
2-Methyl Piperazine (2-MPZ)	A chemical structure showing a piperazine ring with a methyl group attached to one of the nitrogen atoms.	100.16	Sigma-Aldrich Co.	0.95	109-07-9	None
Sulfolane (TMSO ₂)	A chemical structure showing a four-membered thietane-like ring with a sulfur atom at the center and two oxygen atoms at the ends.	120.17	Sigma-Aldrich Co.	0.99	126-33-0	None
Carbon dioxide (CO ₂)	A chemical structure showing the linear molecule CO ₂ .	44.01	Linde India Ltd.	>0.99	-	None

The self-assembly of the surfactants Triton X-114 and Triton X-100 in water solutions at different concentrations and temperatures has been reported,²⁴ where the partition behavior of neutral solutes and micellar structures was studied. The research findings are of great value for extraction and purification through membrane processes using surfactants. The partition behavior of various amino acids at distinct ionization states was predicted successfully using COSMO-RS indicated²⁵ for the extraction of biomolecules using surfactants. A detailed octanol/water partition coefficient prediction through the conceptual application of molecular dynamics and the subsequent input to COSMOmic results in efficient assemblies of complex multiphase fluids are also reported. However, the prediction accuracy depends highly on the i/p molecular structures acquired from molecular dynamics simulations.²⁶ Similar studies can also be performed with respect to the CO₂ capture process of adsorption through membranes.

Further with respect to CO₂ absorption or adsorption, the important properties of understanding are vapor pressure, excess enthalpy, excess Gibb's energy, infinite dilution activity coefficient (IDAC), activity coefficients, chemical potentials, physiochemical properties such as density, viscosity, refractive index, toxicity, biodegradability, thermal stability, corrosion behavior, and CO₂ solubility at a specified temperature and pressure, etc. Thorough knowledge of these properties plays a significant role in selecting a solvent. This is owing to the fact that each of these properties signifies the overall effectiveness of the CO₂ capture process. For instance, if the selected solvent exhibits a high viscosity at the absorption temperature and pressure, the overall pumping costs from the regenerator and absorber columns are expected to be very high. On the other hand, if the chemical potentials of the selected solvents are negative in the selected range of temperature, the solvents will not react with CO₂ chemically at all, leading to merely physisorption in the capture process.

Assessing the possibilities of COSMO-RS for the important parameters of prediction and analysis, the current study is proposed for CO₂ capture through absorption. The nonlinearity

exhibited in the absorption of CO₂ in previously studied solvents^{27,28} suggests that using a quantum calculation method may yield an accurate estimation of various involved thermodynamic properties. The selection of proposed blends is based on an extensive literature survey. The analysis of amine activator 2-methylpiperazine (2-MPZ)^{4,29,30} for enhancement of CO₂ capture is carried out in tertiary amine *N*-methyldiethanolamine (MDEA),^{31,32} physical solvent sulfolane (TMSO₂),^{33,34} and imidazolium-based ionic liquid 1-butyl-3-methyl-imidazolium acetate ([bmim][Ac]).^{35,36} MDEA is reported to exhibit a high CO₂ loading, although it has a low reaction rate. The latter is owing to the fact that MDEA acts only as a weak base to release free OH⁻ that further interacts with CO₂. Further, the reaction of MDEA with CO₂ is less exothermic when compared to primary amines. MDEA additionally offers various advantages such as high thermal and chemical degradation opposition and low solution vapor pressure in comparison to monoethanolamine (MEA) and diethanolamine (DEA).^{37,38} TMSO₂ is also considered for its qualities of high physical absorption capacity, high thermal stability, low heat of absorption, and lower corrosion characteristics.^{33,34} 1-Butyl-3-methylimidazolium acetate, being a room-temperature ionic liquid, offers an insignificantly low vapor pressure and is recognized for its thermal stability and CO₂ capture capacity.

The solvents are chosen in such a manner as to provide molecular and thermodynamic insights into each category of solvents. The base solvents, i.e., MDEA, TMSO₂, and [bmim][Ac], are proposed in the concentration range of 2.5–3.5 mol·kg⁻¹, whereas the concentration range of the activator is varied from 0.5 to 1.5 mol·kg⁻¹. The selected temperature range is 303.15–323.15 K in view of application in absorption phenomena. The variables studied in the respective range of solvents are based on the recommendations in the literature.^{29–39} Various important properties such as σ potential, σ profile, vapor pressure, pure component density and viscosity, infinite dilution activity coefficients, activity coefficients, Gibb's free energy, chemical potential, CO₂ solubility, Henry's law coefficient, etc. have been analyzed through the COSMO-RS theory using

Table 2. Detailed Description of the Mathematical Expressions for the Current Work

sr. no.	property of the system	mathematical equation	description
1	σ profile of the whole system $p_s(\sigma)$	$p_s(\sigma) = \sum_{i \in} x_i \times p_i(\sigma)$	• “ x_i ” is the mole fraction of component “ i ” in the mixture • “ $p^X(\sigma)$ ” is the σ profile of any molecule X • “ $n_i(\sigma)$ ” is the number of distributed segments that has surface charge density σ • “ $A_i(\sigma)$ ” is the segment surface area that has charge density σ • “ A_i ” is the area of the whole surface cavity rooted in the medium
2	σ profile of molecule X	$p^{X_i}(\sigma) = \frac{n_i(\sigma)}{n_i} = \frac{A_i(\sigma)}{A_i}$	• “ $\mu_s(\sigma)$ ” is the chemical potential of a surface segment • “ σ ” is the polarity of the surface under study
3	chemical potential of a surface segment with screening charge density	$\mu_s(\sigma) = -\frac{RT}{a_{\text{eff}}} \ln \left[\int p_s(\sigma') \exp \left(\frac{a_{\text{eff}}}{RT} (\mu_s^*(\sigma') - e(\sigma, \sigma')) \right) d\sigma' \right]$	• “ p_s^* ” is the vapor pressure of the component under study • “ p_{ref} ” is the vapor pressure of the reference component if any considered • “ μ_{gas}^i ” is the chemical potential of the component in the gas phase • “ μ_s^* ” is the chemical potential of the pure component in mixture S • “ R ” is the universal gas constant • “ T ” is the temperature at which the vapor pressure is to be estimated • “ MW_i ” is the molecular weight of the molecule • “ N_A ” is Avogadro’s number • “ \bar{V}_i ” is the corrected molar liquid volume • “ H_i^{MF} ” is the pure component misfit interaction enthalpy • “ H_i^{HB} ” is the hydrogen-bonding enthalpy • “ V_i^{cosmo} ” is the COSMO volume • “ M_i^2 ” is the second σ -moment • “ N_i^{Ring} ” is the number of ring atoms • “ A_i^k ” is the surface area associated with the molecule • “ A_i ” is the surface area • “ M_i^2 ” is the second σ -moment of the compound • “ N_i^{Ring} ” is the number of ring atoms in the compound • “ TS_i ” is the pure component entropy at a specific temperature • $c_{\text{Area}}, c_{\text{M2}}, c_{\text{NRing}}, c_{\text{TS}}$, and c_o are the generic parameters for the QSPR approach for liquid viscosity, with energy values in $\text{kcal}\cdot\text{mol}^{-1}$ and areas in \AA^2
4	vapor pressure	$\frac{p_s^i}{p_{\text{ref}}} = \exp \left[-\frac{(\mu_{\text{gas}}^i - \mu_s^i)}{R \times T} \right]$	• “ γ_i^∞ ” is the activity coefficient of compound “ i ” at infinite dilution • “ μ_i^∞ ” is the pseudo-chemical potential of “ i ” at infinite dilution • “ μ_i^0 ” is the chemical potential of “ i ” in its pure liquid state • “ P^{tot} ” is the total vapor pressure of the mixture
5	pure component density	$\rho_i = \frac{MW_i}{\bar{V}_i \times N_A}$	• “ x_i ” is the mole fraction of the compounds in the liquid phase • “ y_i ” is the mole fraction of compounds in the gas phase
6	corrected molar liquid volume	$\bar{V}_i = (c_{\text{HMF}} \times H_i^{\text{MF}}) + (c_{\text{HHB}} \times H_i^{\text{HB}}) + (c_{\text{cosmo}} \times V_i^{\text{cosmo}}) + (c_{\text{M2}} \times M_i^2) + (c_{\text{NRing}} \times N_i^{\text{Ring}}) + (\sum_k^{\text{Elements}} c_{Ak} \times A_i^k)$	• “ $\alpha_{ij} = \alpha_{ji} = \alpha_j$ ” is the nonrandomness factor that signifies the molecule–molecule or molecule–electrolyte (if any) (default value of 0.3) • “ λ_{ij} ”, “ λ_{ji} ”, “ V_p ”, “ V_p' ”, “ a_{ij} ”, and “ a_{ji} ” are binary interaction parameters of the system under study
7	pure component viscosity (based on a QSPR)	$\ln(\eta i) = (c_{\text{Area}} \times A_i) + (c_{\text{M2}} \times M_i^2) + (c_{\text{NRing}} \times N_i^{\text{Ring}}) + (\sum_k^{\text{Elements}} c_{Ak} \times A_i^k)$	• “ λ_{ij} ”, “ λ_{ji} ”, “ V_p ”, “ V_p' ”, “ a_{ij} ”, and “ a_{ji} ” are binary interaction parameters of the associated constituents
8	activity coefficient at infinite dilution	$\ln \gamma_i^\infty = \frac{\mu_i^\infty - \mu_i^0}{R \times T}$ $\gamma_s^{X_i} = \exp \left(\frac{\mu_s^{X_i} - \mu_{X_i}^{X_i}}{RT} \right)$	• “ λ_{ij} ”, “ λ_{ji} ”, “ V_p ”, “ V_p' ”, “ a_{ij} ”, and “ a_{ji} ” are binary interaction parameters of the system under study
9	COSMO model for VLE	$P^{\text{tot}} = \sum_i P_{\text{vap}}^{X_i} x_i y_s^{X_i}$ $\gamma_i = \frac{P_{\text{vap}}^{X_i} x_i y_s^{X_i}}{P^{\text{tot}}}$	• “ x_i ” is the mole fraction of the compounds in the liquid phase • “ y_i ” is the mole fraction of compounds in the gas phase
10	nonrandom two-liquid (NRTL) model	$\ln(\gamma_i) = \frac{\sum_j x_j \tau_{ji} G_{ji}}{\sum_k x_k G_{ki}} + \sum_j \frac{x_i G_{ij}}{\sum_k x_k G_{kj}} \left[\tau_{ij} - \frac{\sum_m x_m \tau_{mj} G_{mj}}{\sum_k x_k G_{kj}} \right]$ $G_{ij} = \exp(-\alpha_{ij} \tau_{ij})$	• “ $\alpha_{ij} = \alpha_{ji} = \alpha_j$ ” is the nonrandomness factor that signifies the molecule–molecule or molecule–electrolyte (if any) (default value of 0.3) • “ λ_{ij} ”, “ λ_{ji} ”, “ V_p ”, “ V_p' ”, “ a_{ij} ”, and “ a_{ji} ” are binary interaction parameters of the system under study
11	WILSON model	$\ln(\gamma_i) = 1 - \ln(\sum_k x_k \lambda_{ik}) - \sum_j \frac{x_i \lambda_{ji}}{\sum_k x_k \lambda_{jk}}$ $\Omega_{ij} = \lambda_{ji} = \frac{V_i}{V_j} \exp \left[-\frac{a_{ji}}{RT} \right]$	• “ λ_{ij} ”, “ λ_{ji} ”, “ V_p ”, “ V_p' ”, “ a_{ij} ”, and “ a_{ji} ” are binary interaction parameters of the system under study

Table 2. continued

sr. no.	property of the system	mathematical equation	description
12	UNIQUAC 4 model	$\ln(\gamma_i) = \ln(\gamma_i^C) + \ln(\gamma_i^R)$ $\ln(\gamma_i^C) = \ln\left(\frac{\phi_i}{x_i}\right) + \frac{z}{2}q_i \ln\left(\frac{\Theta_i}{\phi_i}\right) + l_i - \frac{\phi_i}{x_i} \sum_j x_j l_j$ the parametric equations are as follows $\phi_i = \frac{x_i r_i}{\sum_j r_j x_j}$ $\Theta_i = \frac{x_i q_i}{\sum_j q_j x_j}$ $l_i = \frac{z}{2}(r_i - q_i) - (r_i - 1)$ the enthalpy interactions among various constituents in the UNIQUAC 4 model are quantified by the residual contribution in the calculation of the activity coefficient; the mentioned term is described as $\ln(\gamma_i^R) = q_i \left[1 - \ln\left(\sum_j \Theta_j \tau_{ji} \right) - \sum_j \frac{\Theta_j \tau_{ij}}{\sum_k \Theta_k \tau_{kj}} \right]$ enthalpy, being closely related to temperature, the residual contribution of binary interaction major parameters " τ_{ij} " is further taken as an inverse logarithm function of temperature and is given as $\ln(\tau_{ij}) = -\frac{\Delta u_{ij}}{RT} = -\frac{a_{ij}}{T}$ the compound-specific UNIQUAC volume and surface area parameters are presented as $r_i = \frac{s_i V_i^{\text{COSMO}}}{30}$ $q_i = \frac{s_i A_i^{\text{COSMO}}}{40}$	• "ln(γ_i^C)" is the combinatorial contribution signifying the entropic size and shape transformations of the compounds • " Φ_i " and " Θ_i " are the normalized volume and surface area fraction of species " i " in the blended solvent • " x_i " is the mole fraction • " r_i " is the volume • " q_i " is the surface area for each individual species ($\tau_{ji} \neq \tau_{ij}$)
13	gas solubility	$p_j = p_j^0 \times x_j \times \gamma_j$	• " p_j^0 " is the vapor pressure of the pure compound • " γ_j " is the activity coefficient • " x_j " is the mole fraction • " p_j " is the partial pressure of compound " j " • " H_j^s " is Henry's law coefficient of compound " j " in solvent " s " • " $\mu_j^{s,\infty}$ " is the ideal gas-phase chemical potential • " μ_j^{gas} " is the infinite dilution state chemical potential • " $\gamma_j^{s,\infty}$ " is the activity coefficient at infinite dilution • " p_j^p " is the pure compound vapor pressure
14	Henry's law coefficient	$H_j^s = \exp\left[\frac{(\mu_j^{s,\infty} - \mu_j^{\text{gas}})}{R \times T}\right] = \gamma_j^{s,\infty} \times p_j^p$	• " p_j^0 " is the vapor pressure of the pure compound • " γ_j " is the activity coefficient • " x_j " is the mole fraction • " p_j " is the partial pressure of compound " j " • " H_j^s " is Henry's law coefficient of compound " j " in solvent " s " • " $\mu_j^{s,\infty}$ " is the ideal gas-phase chemical potential • " μ_j^{gas} " is the infinite dilution state chemical potential • " $\gamma_j^{s,\infty}$ " is the activity coefficient at infinite dilution • " p_j^p " is the pure compound vapor pressure

COSMOtherm to evaluate the applicability of the proposed solvents.

2. COMPUTATIONAL METHODS AND THEORY

The molecules under study, i.e., N-methyldiethanolamine (MDEA), sulfolane (TMSO₂), 1-butyl-3-methylimidazole, cation ([bmim]), acetate anion ([Ac]), H₂O, CO₂, and 2-methylpiperazine (2-MPZ), were selected within COSMOtherm (COSMOlogic GmbH, Leverkusen, Germany). Single conformers with the least ground-state energy were selected for each of the molecular compounds obtained with BP-TZVPD-FINE-level COSMO calculations that incorporate a full geometry optimization by density functional theory (DFT) using the Becke and Perdew (BP) functional with the triple- ζ valence polarized (TZVP) basic set. The detailed specifications of the chemicals for the experimental work are presented in Table 1. The analysis of σ surface, σ potential, and vapor–liquid equilibrium and estimation of vapor pressure, pure component density and viscosity, infinite dilution activity coefficients, CO₂ solubility, Henry's law coefficient, and pK_a values are carried

out over a wide range of temperatures using the respective modules within COSMOtherm. For pK_a calculations, the respective protonated structures of the molecules were developed using TURBOMOLE. All of the estimated values have been presented up to three significant digits after the decimal.

3. RESULTS AND DISCUSSION

The detailed mathematical relationships of various studied parameters with chemical potential are presented in Table 2.⁴⁰ The conforming significance of the simulated properties has been conversed alongside the analysis results.

3.1. σ Profile and σ Potential Analysis. The intermolecular interactions of the selected solvents among all of the constituents along with CO₂ contribute largely toward CO₂ solubility. This further hinges on the associated shape, size, polarity, and type of molecules. Chemical potential " μ " of any species in a solution is evaluated using screening charge density " σ " on the surface of molecules through the COSMO-RS theory within three major norms: (i) the liquid state is incompressible, (ii) all fragments of molecular surfaces can be in interaction

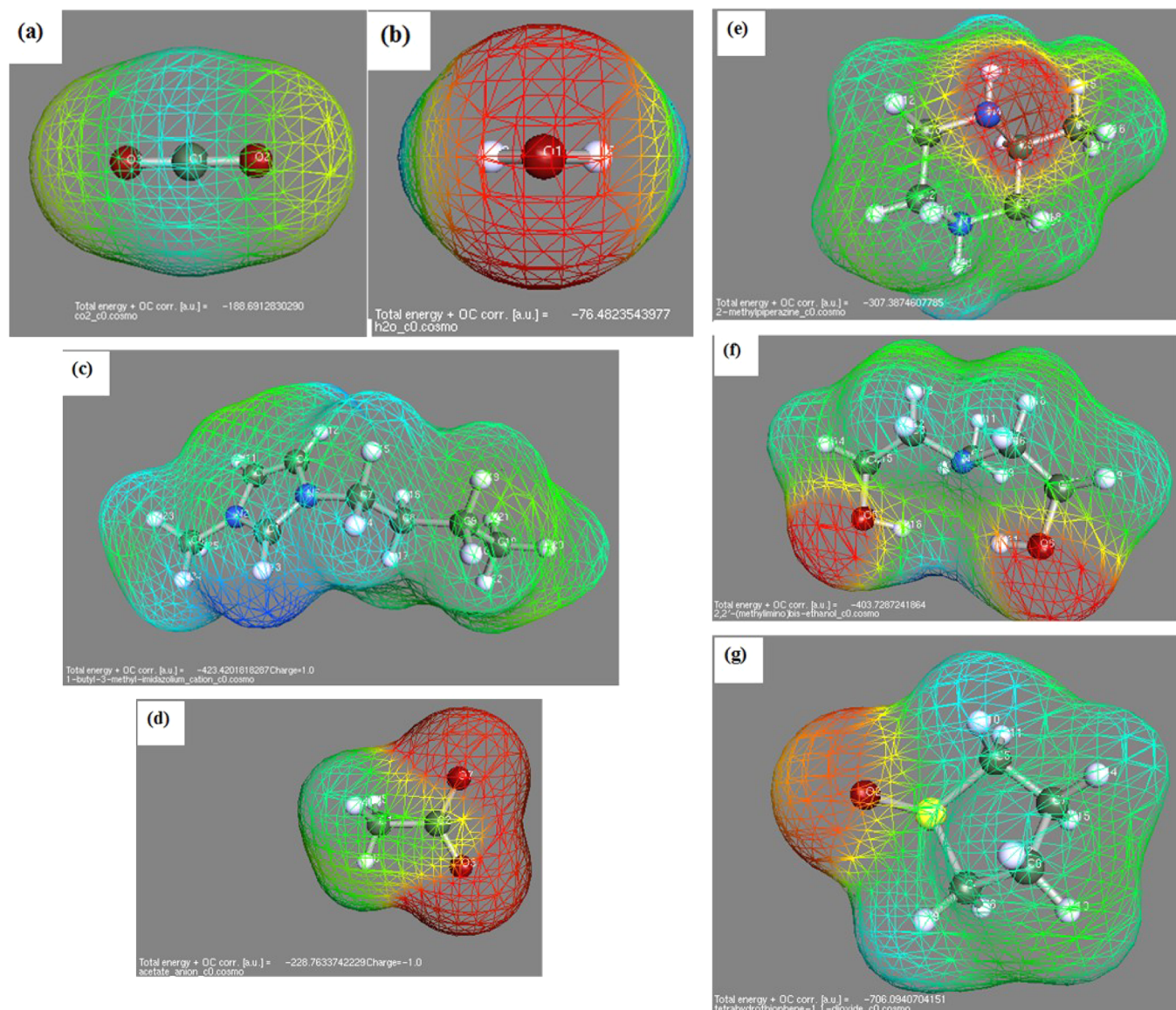


Figure 1. σ surface of (a) CO_2 , (b) H_2O , (c) $[\text{bmim}]$ cation, (d) $[\text{Ac}]$ acetate anion, (e) 2-MPZ, (f) MDEA, and (g) TMSO_2 .

with one another, and (iii) individual pairwise interactions of molecular surface areas are permitted. This screening charge density also helps in understanding electrostatic interaction, hydrogen-bonding energy, dispersion, etc. The σ -profile of any molecule is obtained through the weighted sum of the profiles of all of its included components. σ profiles also signify the spreading of screening charge density (σ) of molecules. This distribution is carried out in three categories: (a) nonpolar region ($-0.0084 \text{ e}\cdot\text{\AA}^{-2} < \sigma < 0.0084 \text{ e}\cdot\text{\AA}^{-2}$), hydrogen-bond donor (HBD) region ($\sigma < -0.0084 \text{ e}\cdot\text{\AA}^{-2}$), and hydrogen-bond acceptor (HBA) region ($\sigma > 0.0084 \text{ e}\cdot\text{\AA}^{-2}$).

The σ surfaces of H_2O , $[\text{bmim}]$ cation, $[\text{Ac}]$ anion, CO_2 , 2-MPZ, MDEA, and TMSO_2 are shown in Figure 1 along with the energy associated with each molecule. The zones in the figure can be explained as follows. Red: hydrogen-bond acceptor; blue: hydrogen-bond donor; and green: nonpolar section of the molecule. Single conformers with the least ground-state energy associated with the molecule were considered for the current work.

The σ profile and the corresponding σ potential for the molecules functional to majorly chemical potential are shown

in Figure 2. These properties define the attraction of selected solvents with the desired solute, thereby determining the extent of possible separation.

The negative polarities of any molecule are indicated by positive screening charge density in a σ -scale and vice versa.⁴¹ The least σ surface was obtained for H_2O in the extensive range of $-0.02 \text{ e}\cdot\text{\AA}^{-2}$, and $+0.02 \text{ e}\cdot\text{\AA}^{-2}$ specifies the positive and negative polarities of the associated atoms in the H_2O molecule. Successively, it can also be seen from Figure 2a that key portions of σ charge densities of the $[\text{bmim}]$ cation, TMSO_2 , MDEA, and 2-MPZ are negative and those for CO_2 and the $[\text{Ac}]$ anion are positive in nature. Further, the peak intensities of MDEA and 2-MPZ are very competitive with each other, indicating the possible high CO_2 solubility offered by both. Also, if the peaks of TMSO_2 are analyzed, it can be perceived to have a positive and negative σ charge density with two sharp peaks. The higher peak is, however, present on the negative side. It can thus be concluded that as CO_2 and selected solvents present different charge densities, the selected solvents could provide good CO_2 absorption. This conclusion is in agreement with the fact that the negative surface pieces of

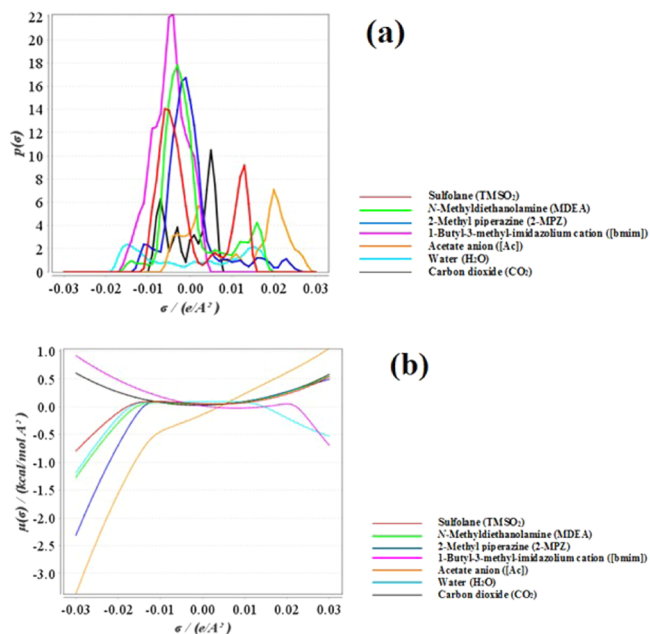


Figure 2. COSMOtherm generated (a) σ profile and (b) σ potential of MDEA, TMSO_2 , $[\text{bmim}][\text{Ac}]$ cation, acetate $[\text{Ac}]$ anion, H_2O , CO_2 , and 2-MPZ.

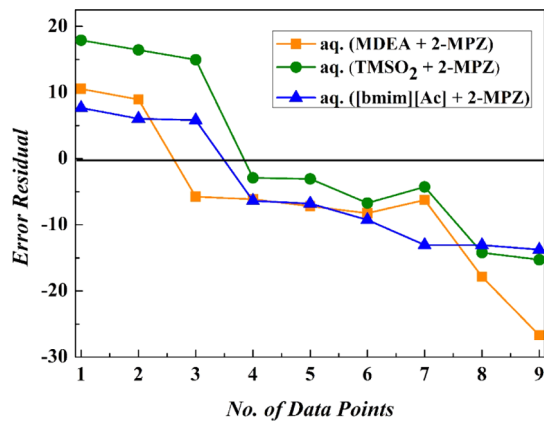


Figure 3. Residual plot of vapor pressure experimental and COSMO predicted for aq (MDEA + 2-MPZ), aq (TMSO_2 + 2-MPZ), and aq ($[\text{bmim}][\text{Ac}]$ + 2-MPZ) systems.

[bmim], 2-MPZ, TMSO_2 , and MDEA can react essentially with the positive surface pieces of CO_2 .⁴² Although the [bmim] cation is seen to provide the highest negative surface, on

combining it with the associated $[\text{Ac}]$ cations' positive surface, it results in overall less polarity available in comparison to MDEA and 2-MPZ.

The intermolecular interaction of a solvent toward the molecular surface that it comes in contact with polar or nonpolar behavior can be qualitatively discussed in terms of the σ potential.⁴³ The positive σ potential of CO_2 over the studied charge density of -0.03 to $+0.03 \text{ e}\cdot\text{\AA}^{-2}$ indicates its capability as a H-bond acceptor (Figure 2b). The σ potential behavior of CO_2 is almost symmetrical and concave in nature over the entire charge density. On the contrary, the parameter is asymmetrical for $[\text{bmim}]$, $[\text{Ac}]$, 2-MPZ, MDEA, and TMSO_2 , leaning more to the negative side of charge density. Additionally, only the $[\text{bmim}]$ cation is associated with a positive σ potential in the negative surface charge density region. The molecules signifying a $-ve$ σ potential act as H-bond donors, whereas the $+ve$ σ potential suggests that CO_2 is a H-bond acceptor. However, understanding the $[\text{bmim}]$ cation alone does not provide any technical application since, in the present study, it is associated with the $[\text{Ac}]$ anion. Combining the chemical potentials of both the $[\text{bmim}]$ cation and the $[\text{Ac}]$ anion leads to the overall negative charge density, proposing it to be a H-bond donor. The formation or loss of a H bond is usually at the S, N, or O atoms of any molecules. At a molecular level, the possible interaction of CO_2 with any chosen solvent depends highly on the H-bond acceptor or donor capacity. The interaction strength of CO_2 can hence be determined with the order as MDEA > 2-MPZ > $[\text{bmim}][\text{Ac}]$ > TMSO_2 > H_2O . At a lab or plant scale, the same concept is understood by the reaction mechanism of zwitterions, proton exchange reactions, and formation or dissolution of bicarbonates, unstable/stable bicarbamates, and dicarbamates.^{44,45}

3.2. Vapor Pressure Analysis. The potential applications of any solvent in diverse fields of chemical engineering depend on many important characteristics such as thermal and mechanical stability, low degradation and toxicity levels, the extent of biodegradation offered, recyclability, vapor pressures, etc. Among these many essential features, vapor pressure is considered to be very important for the CO_2 capture process. This is due to the fact that any solvent exhibiting high vapor pressure will lead to huge losses during regeneration. Also, if the vapor pressure is too high, the solubility of CO_2 or other acid solute gases decreases at high temperatures. The latter is because, at high temperatures, the diffusivity is expected to increase considerably. On the other hand, if the vapor pressure is too low, e.g., in the case of pure ionic liquids, the diffusion is also too less at low temperatures. Hence, an optimum vapor pressure is desired

Table 3. Comparison of Experimental and COSMO Predicted Vapor Pressure of Aq (MDEA + 2-MPZ), Aq (TMSO_2 + 2-MPZ), and Aq ($[\text{bmim}][\text{Ac}]$ + 2-MPZ) Systems

system	concentration ($\text{mol}\cdot\text{kg}^{-1}$)	T (K)	303.15	303.15	313.15	313.15	323.15	323.15	% AAD
		experimental	predicted	experimental	predicted	experimental	predicted		
aq (MDEA + 2-MPZ)	(3.509 + 0.509)	48.9	38.412	62.1	68.191	109.6	115.879	16.255	
	(3.017 + 1.008)	47.6	38.628	61.4	68.545	98.6	116.437		
	(2.502 + 1.509)	33.1	38.856	60.7	68.917	90.3	117.023		
aq (TMSO_2 + 2-MPZ)	(3.501 + 0.509)	56.5	38.624	65.5	68.393	111.7	115.958	15.777	
	(3.012 + 1.008)	55.2	38.709	65.5	68.552	102.0	116.243		
	(2.500 + 1.509)	53.8	38.829	62.1	68.767	101.4	116.614		
aq ($[\text{bmim}][\text{Ac}]$ + 2-MPZ)	(3.507 + 0.509)	45.5	37.839	60.7	67.039	100.7	113.719	13.407	
	(3.002 + 1.008)	44.1	38.074	60.7	67.454	101.4	114.423		
	(2.510 + 1.509)	44.1	38.306	58.6	67.863	101.4	115.116		

Table 4. COSMO Predicted Antoine Equation Coefficients in Aq (MDEA + 2-MPZ), Aq (TMSO₂ + 2-MPZ), and Aq ([bmim][Ac] + 2-MPZ) Systems^a

system	concentration (mol·kg ⁻¹)	A	B	C
aq (MDEA + 2-MPZ)	(3.509 + 0.509)	18.101	3495.889	-61.252
	(3.017 + 1.008)	18.106	3498.779	-61.057
	(2.502 + 1.509)	18.112	3501.691	-60.853
aq (TMSO ₂ + 2-MPZ)	(3.501 + 0.509)	18.072	3495.181	-60.728
	(3.012 + 1.008)	18.086	3500.407	-60.568
	(2.500 + 1.509)	18.099	3504.717	-60.426
aq ([bmim][Ac] + 2-MPZ)	(3.507 + 0.509)	18.065	3498.714	-60.718
	(3.002 + 1.008)	18.083	3504.428	-60.511
	(2.510 + 1.509)	18.097	3508.562	-60.358

^aln(P) = A - $\frac{B}{(T+C)}$ (P is in millibar and T is in kelvin).

Table 5. Comparison of Experimental and COSMO Predicted Density (ρ , kg·m⁻³) of Pure MDEA, TMSO₂, 2-MPZ, and [bmim][Ac]

data	system							
	MDEA		2-MPZ		TMSO ₂		[bmim][Ac]	
	ρ_{exp}	ρ_{pred}	ρ_{exp}	ρ_{pred}	ρ_{exp}	ρ_{pred}	ρ_{exp}	ρ_{pred}
T (K)								
298.15	1036.8	984.816	875.5	995.703	1013.3	1346.294	1052.1	1067.123
303.15	1032.9	979.811	872.7	991.028	1008.1	1340.947	1049.1	1063.032
308.15	1029.2	974.833	869.8	986.363	1004.3	1335.579	1045.9	1058.923
313.15	1025.4	969.882	866.9	981.711	1000.4	1330.191	1043.0	1054.796
318.15	1020.9	964.957	863.9	977.069	996	1324.783	1040.0	1050.652
323.15	1017.7	960.059	860.9	972.441	992.8	1319.356	1037.0	1046.493
328.15	1012.9	955.187	857.8	967.824	988.4	1313.911	1034.1	1042.318
333.15	1009.1	950.341	854.7	963.220	985.1	1308.450	1031.1	1038.129
% AAD	5.439		13.189		32.936		1.067	

Table 6. Comparison of Experimental and COSMO Predicted Viscosity (η , mPa·s) of Pure MDEA, 2-MPZ, and TMSO₂

data	system					
	MDEA		2-MPZ		TMSO ₂	
	η_{exp}	η_{pred}	$\eta_{\text{pred,aspen}}$	$\eta_{\text{pred,COSMO}}$	η_{exp}	η_{pred}
T (K)						
298.15	77.75	3.839	0.47	4.462	10.28	2.917
303.15	56.26	3.459	0.46	4.005	10.22	2.648
308.15	46.47	3.127	0.45	3.607	9.06	2.411
313.15	34.66	2.836	0.43	3.259	7.84	2.202
318.15	28.67	2.580	0.42	2.954	6.58	2.016
323.15	23.29	2.354	0.41	2.686	6.18	1.851
328.15	17.42	2.154	0.40	2.449	5.19	1.705
333.15	14.55	1.976	0.39	2.239	4.88	1.573
% 10 ⁻² × AAD	0.911		6.405		0.707	

Table 7. COSMO Predicted Activity Coefficients of MDEA, TMSO₂, and 2-MPZ at Infinite Dilution in Water

T (K)	298.15	303.15	308.15	313.15	318.15	323.15	328.15	333.15
MDEA	0.671	0.823	0.997	1.193	1.411	1.650	1.909	2.186
TMSO ₂	4.255	4.493	4.719	4.931	5.126	5.304	5.462	5.601
2-MPZ	0.246	0.305	0.375	0.455	0.549	0.655	0.774	0.908

to achieve both absorption and regeneration cost-effectively. Considering that the initial screening of solvents for any application requires major experimental investigations, the cost-effectiveness can be reduced, provided that the proficient prediction methods for such properties are available. In the same line, many researchers have proposed vapor pressure estimation through traditional or modified thermodynamic equations such as PR-EoS, UNIFAC, UNIFAC-Lei, etc.^{46–50} The efficacy of

any such model depends on the number of assumptions made during calculations, in addition to the number of thermodynamic parameters calculated. For the current work, quantum calculations through COSMO-RS are carried out including the combinatorial and residual parametric contributions of the molecules under study. The vapor pressures are estimated using the boiling points of individual pure constituents of the systems under study as the reference point. The variance in the

Table 8. COSMO Predicted NRTL Parameters for the Activity Coefficients in (H_2O (1) + MDEA (2) + 2-MPZ (3)), (H_2O (1) + TMSO_2 (2) + 2-MPZ (3)), and (H_2O (1) + [bmim][Ac] (2) + 2-MPZ (3)) Systems

system	aq (MDEA + 2-MPZ)			aq (TMSO_2 + 2-MPZ)			aq ([bmim][Ac] + 2-MPZ)			
	T (K)	303.15	313.15	323.15	303.15	313.15	323.15	303.15	313.15	323.15
A	0.3	0.3	0.3	0.3	0.3	0.3	0.3	0.3	0.3	0.3
τ_{12}	-0.952	-0.863	-0.753	0.376	0.456	1.336	-1.918	-1.839	-1.760	
τ_{13}	0.803	0.975	1.228	0.920	1.207	5.479	0.055	0.099	0.151	
τ_{21}	1.999	1.900	1.761	1.580	1.388	0.533	-3.167	-3.053	-2.943	
τ_{23}	1.231	1.150	1.052	0.740	0.643	0.663	1.484	1.381	1.289	
τ_{31}	-2.167	-2.108	-2.077	-2.267	-2.229	-2.727	-2.052	-1.895	-1.746	
τ_{32}	0.016	-0.018	-0.029	1.686	1.600	1.287	1.416	1.393	1.375	
RMSD	0.329	0.309	0.291	0.394	0.371	0.331	0.531	0.493	0.459	

Table 9. COSMO Predicted WILSON Parameters for the Activity Coefficients in (H_2O (1) + MDEA (2) + 2-MPZ (3)), (H_2O (1) + TMSO_2 (2) + 2-MPZ (3)), and (H_2O (1) + [bmim][Ac] (2) + 2-MPZ (3)) Systems

system	aq (MDEA + 2-MPZ)			aq (TMSO_2 + 2-MPZ)			aq ([bmim][Ac] + 2-MPZ)			
	T (K)	303.15	313.15	323.15	303.15	313.15	323.15	303.15	313.15	323.15
λ_{12}	0.223	0.221	0.224	0.210	0.232	0.258	11.673	10.800	10.011	
λ_{13}	4.132	3.878	3.658	4.199	3.944	3.719	4.721	4.251	3.838	
λ_{21}	1.817	1.731	1.641	0.518	0.525	0.528	5.144	4.904	4.675	
λ_{23}	0.865	0.918	0.964	0.223	0.250	0.276	0.376	0.381	0.384	
λ_{31}	1.209	1.103	0.994	1.259	1.126	0.994	1.247	1.173	1.098	
λ_{32}	0.315	0.329	0.347	0.275	0.319	0.361	0.087	0.099	0.112	
a_{12}	-0.199	-0.201	-0.215	-0.061	-0.125	-0.196	-2.487	-2.521	-2.553	
a_{13}	-1.878	-1.901	-1.924	-1.888	-1.911	-1.934	-1.958	-1.958	-1.955	
a_{21}	0.744	0.798	0.858	1.397	1.434	1.476	0.020	0.051	0.083	
a_{23}	0.167	0.136	0.109	0.882	0.838	0.801	0.573	0.584	0.596	
a_{31}	0.909	0.996	1.095	0.885	0.983	1.095	0.890	0.958	1.031	
a_{32}	0.617	0.608	0.595	0.802	0.735	0.679	1.487	1.456	1.424	
v_1	25.855	25.855	25.855	25.855	25.855	25.855	25.855	25.855	25.855	
v_2	161.363	161.363	161.363	136.050	136.050	136.050	137.507	137.507	137.507	
v_3	141.349	141.349	141.349	141.350	141.349	141.349	141.349	141.349	141.349	
RMSD	0.346	0.320	0.299	0.404	0.378	0.355	0.749	0.687	0.630	

correlated and experimental values of the parameters under study is obtained through calculation of deviation using the following equation

$$\% \text{AAD} = \frac{100}{N} \times \sum_{i=1}^N \frac{|Y_i^{\text{exp}} - Y_i^{\text{mod}}|}{Y_i^{\text{exp}}} \quad (1)$$

where N , Y_i^{exp} , and Y_i^{mod} indicate the number of data points, experimental value, and modeled or COSMOtherm estimated value of any variable, respectively.

The vapor pressures of aqueous (aq) (MDEA + 2-MPZ), aq (TMSO_2 + 2-MPZ), and aq ([bmim][Ac] + 2-MPZ) have been measured using the validated experimental methodology of our previous work.⁵¹ The measurements have been carried out at 303.15, 313.15, and 323.15 K and a total solvent concentration of 4.0 mol·kg⁻¹. The activator 2-MPZ concentration is varied from 0.5 to 1.5 mol·kg⁻¹ in the studied solvents. Further, estimation of Antoine equation coefficients is carried out in the temperature range of 298.15–333.15 K. The obtained outcomes are presented in Figure 3 and Tables 3 and 4. The deviations among the experimental and predicted values of vapor pressures for aq (MDEA + 2-MPZ), aq (TMSO_2 + 2-MPZ), and aq ([bmim][Ac] + 2-MPZ) are 16.255, 15.777, and 13.407%, respectively. The obtained deviation through the COSMO-RS theory is quite less when compared to the analytical expressions used for similar estimations.^{52,53} Nonetheless, the obtained deviations can be attributed to the uncertainties associated with

the experimental procedure inclusive of variations in temperature, pressure, and compositions, which have been retained constant throughout the experimentation. Also, while performing quantum calculations, such macroscopic deviations are not considered.

3.3. Estimation of Pure Component Density and Viscosity. The experimental analysis of pure component density and viscosity has been reported by many researchers for different purposes in carbon capture systems, mainly for estimation of kinetic parameters and pumping costs,^{54,55} concise designing of absorption–stripper columns,⁵⁶ understanding the nonideal behavior through analysis of viscosity deviation or excess molar properties,⁵⁷ etc. In the present work, pure component density and viscosity are estimated through the quantitative structure–property relationship (QSPR) approach, which consists of many inherent properties of the involved molecules (Table 2). The pure component density and viscosity measurements have been carried out using a density and sound velocity meter (DSA 5000 M, Anton Paar, Austria) and an Anton Paar AMVn rolling ball viscometer with the standard uncertainties of $u(T) = 0.01$ K, $u(P) = 0.2$ kPa, $u(\rho) = 0.5$ kg·m⁻³, and $u(\eta) = 0.07$ mPa·s. The adopted detailed methodology can be referred to from our previous work.⁵¹

A comparison of the experimental and COSMO estimated density and viscosity of the involved chemical species is presented in Tables 5 and 6. For the case of 2-MPZ, since it is in crystalline form, the experimental measurement was difficult and hence viscosity was estimated using Aspen plus⁵⁸ and

Table 10. COSMO Predicted UNIQUAC 4 Parameters for the Activity Coefficients in (H_2O (1) + MDEA (2) + 2-MPZ (3)), (H_2O (1) + TMSO_2 (2) + 2-MPZ (3)), and (H_2O (1) + [bmim][Ac] (2) + 2-MPZ (3)) Systems

systems	aq (MDEA + 2-MPZ)			aq (TMSO_2 + 2-MPZ)			aq ([bmim][Ac] + 2-MPZ)		
	T (K)	303.15	313.15	323.15	303.15	313.15	323.15	303.15	313.15
q_1	1.653	1.622	1.579	2.223	2.014	1.838	7.058	6.572	6.086
q_2	1.692	1.705	1.707	0.996	0.983	0.964	19.599	18.544	17.453
q_3	9.946	9.665	9.349	11.529	10.621	9.920	30.774	28.501	26.338
r_1	1.086	1.066	1.038	1.461	1.324	1.208	5.639	5.251	4.863
r_2	2.232	2.249	2.253	1.279	1.262	1.237	24.320	23.012	21.658
r_3	12.801	12.439	12.034	14.839	13.671	12.768	39.608	36.684	33.899
τ_{12}	0.108	0.101	0.100	0.117	0.127	0.136	2.240	2.278	2.322
τ_{13}	2.241	2.132	2.026	1.729	1.689	1.624	1.447	1.443	1.438
τ_{21}	4.717	4.540	4.341	2.823	2.724	2.625	1.012	0.984	0.955
τ_{23}	1.454	1.447	1.439	1.087	1.084	1.072	1.466	1.449	1.433
τ_{31}	0.849	0.849	0.845	1.394	1.327	1.271	1.183	1.166	1.148
τ_{32}	0.245	0.261	0.275	0.025	0.030	0.034	0.549	0.557	0.565
u_{12}	1.341	1.426	1.478	1.295	1.286	1.282	-0.486	-0.512	-0.541
u_{13}	-0.486	-0.471	-0.453	-0.329	-0.326	-0.311	-0.223	-0.228	-0.233
u_{21}	-0.935	-0.942	-0.943	-0.625	-0.624	-0.619	-0.007	0.010	0.029
u_{23}	-0.225	-0.230	-0.234	-0.050	-0.050	-0.045	-0.230	-0.231	-0.231
u_{31}	0.098	0.102	0.109	-0.200	-0.176	-0.154	-0.101	-0.096	-0.089
u_{32}	0.848	0.836	0.829	2.213	2.181	2.175	0.362	0.364	0.367
a_{12}	675.017	717.561	743.797	651.785	646.952	645.321	-244.517	-257.853	-272.239
a_{13}	-244.652	-237.117	-228.163	-166.034	-164.243	-156.605	-112.064	-114.933	-117.345
a_{21}	-470.235	-473.772	-474.405	-314.656	-313.838	-311.885	-3.667	5.039	14.787
a_{23}	-113.390	-115.781	-117.811	-25.154	-25.191	-22.549	-115.886	-116.072	-116.211
a_{31}	49.453	51.136	54.603	-100.711	-88.555	-77.544	-50.919	-48.067	-44.636
a_{32}	426.718	420.757	416.955	1113.699	1097.438	1094.228	182.039	183.115	184.581
RMSD	0.279	0.262	0.247	0.325	0.309	0.295	0.375	0.353	0.333

COSMOtherm and a comparison of the two has been presented. The least deviations observed are with respect to the viscosity of TMSO_2 and density of [bmim][Ac], i.e., 0.707 × 10² and 1.067%, respectively. A major reason for this huge deviation, especially with respect to viscosity, is owing to the fact that the structural relationship utilized for the prediction of pure component properties, i.e., QSPR, is assumed to be independent of temperature, which is usually not due to non-Newtonian and nonideal liquid systems. However, similar observations are also reported elsewhere.⁵⁹ As a matter of fact, it can be concluded from the present comparison of experimental and COSMO-computed values of density and viscosity that the estimation is not accurate for both the properties. Further, the prediction of pure component density and viscosity does not get reflected in other evaluations for the reason that, as indicated in Table 2, the other properties are calculated as a function of chemical potential. Hence, effective prediction of chemical potential results in accurate predictions of the properties under consideration such as vapor pressure, except pure component density and viscosity.

3.4. Infinite Dilution Activity Coefficients. The magnitude of nonideality in liquid solutions is often in terms of infinite dilution activity coefficients (IDACs). Since the solvents associated with absorption of CO_2 and consequently the same solvent for desorption while releasing CO_2 from it are expected to show nonideality behavior, such nonidealities are also variously expressed in terms of property deviations such as density and viscosity deviations from ideality. A few important thermodynamic properties, for instance, partition coefficient, separation factors, and Henry's law coefficient, are also dictated by activity coefficients. However, the experimental calculation of IDACs is difficult and expensive. Hence, a preliminary

analysis through the apposite prediction method is of huge interest.^{60–62} The estimation of IDACs of aqueous, nonaqueous, organic, or ionic liquid systems, through COSMO-RS, is reported in the literature to be very efficient owing to the reason the same being evaluated in the absenteeism of mean-field approximation.⁶³ The nonpolarity or active polarity of a compound is decided by the higher or lower value of IDACs in the system (Table 2). Table 7 presents the COSMO predicted infinite dilution activity coefficients of MDEA, 2-MPZ, and TMSO_2 in H_2O as a function of temperature in the range of 298.15–333.15 K. With an increase in the temperature, IDACs of MDEA, TMSO_2 , and 2-MPZ in water were found to increase. Although the IDACs values for MDEA and 2-MPZ are very low in comparison to the TMSO_2 values, for the currently studied compounds, all of the IDACs are greater or less than unity, indicating the highly nonideal behavior of such systems.⁴³

3.5. Vapor–Liquid Equilibrium Relationship of Aq (MDEA + 2-MPZ), Aq (TMSO_2 + 2-MPZ), and Aq ([bmim][Ac] + 2-MPZ). At a specific temperature and pressure, the extent of reaction resulting in formation of products or scattering of various constituents is dependent on the chemical potential and subsequently on the Gibbs' free energy. Further, the maximum gas solubility at equilibrium is also dependent on the values of the activity coefficients of the solvent. The chemical potential is also considered a sum total of various energies as well as factors affecting the energies such as internal, density, temperature, enthalpy, etc., of any molecule. This indicates the dependency of acid–gas separations at a molecular level on the thermodynamic properties such as chemical potential, enthalpy, Gibbs' free energy, etc.

Henceforth, the vapor–liquid equilibrium of the ternary mixtures of aq (MDEA + 2-MPZ), aq (TMSO_2 + 2-MPZ), and

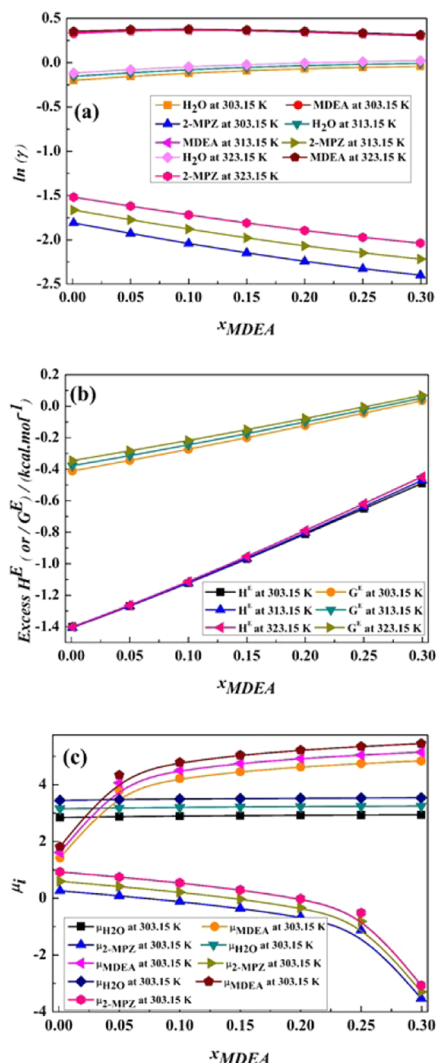


Figure 4. COSMO predicted (a) activity coefficient, (b) excess enthalpy and Gibbs's free energy, and (c) chemical potential as a function of mole fraction of MDEA for the aq (MDEA + 2-MPZ) system at $x_{\text{H}_2\text{O}} = 0.7$.

aq ([bmim][Ac] + 2-MPZ) related to the nonlinear behavior of the various constituents involved is determined using the COSMO-RS theory. The VLE estimated through COSMO is based on the vapor pressure and activity coefficients of individual pure constituents in the mixture (Table 2). The VLE is additionally modeled using NRTL, WILSON, and UNIQUAC 4 models. The obtained VLE data is presented in the form of activity coefficients, excess Gibbs free energy, excess enthalpy, chemical potential, and individual partial pressures associated with each system at 303.15, 313.15, and 323.15 K. The total pressures of the aq (MDEA + 2-MPZ), aq (TMSO_2 + 2-MPZ), and aq ([bmim][Ac] + 2-MPZ) systems are taken to be 0–124 mbar. The difference between the COSMO and NRTL/WILSON/UNIQUAC 4 model predicted activity coefficients is calculated in terms of the root-mean-square deviation (RMSD) using the following equation

$$\text{RMSD} = \sqrt{\frac{\sum_{i=1}^n (y_{\text{COSMO}} - y_i)^2}{n}} \quad (2)$$

where y_{COSMO} is the COSMO predicted property and y_i is the NRTL, WILSON, or UNIQUAC predicted property value.

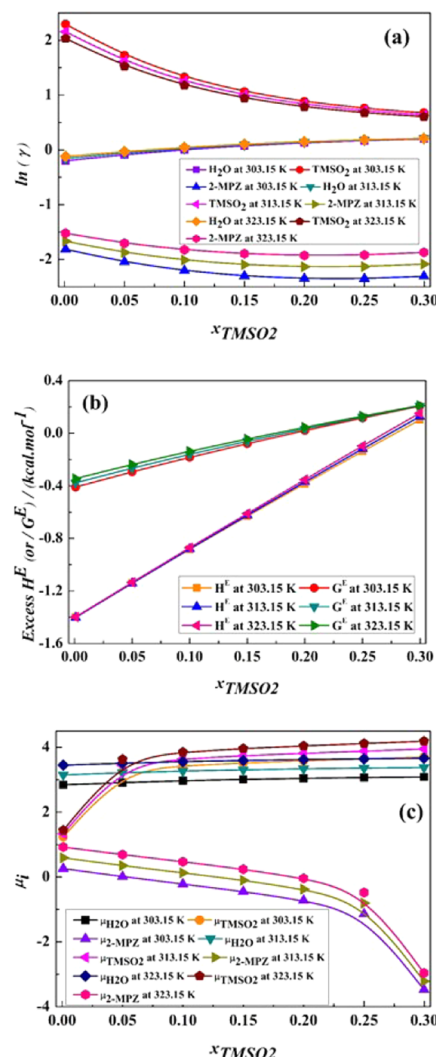


Figure 5. COSMO predicted (a) activity coefficient, (b) excess enthalpy and Gibbs's free energy, and (c) chemical potential as a function of mole fraction of TMSO_2 for the aq (TMSO_2 + 2-MPZ) system at $x_{\text{H}_2\text{O}} = 0.7$.

The activity coefficients and binary interaction parameters for NRTL, WILSON, and UNIQUAC 4 models of the systems under study were estimated and are presented in Tables 8, 9, and 10, respectively. The majority of the binary interaction parameters of the studied systems are found to be different because the systems are asymmetric, i.e., $\tau_{ji} \neq \tau_{ij}$.^{64,65}

The obtained results are presented graphically for aq (MDEA + 2-MPZ), aq (TMSO_2 + 2-MPZ), and aq ([bmim][Ac] + 2-MPZ) in Figures 4, 5, and 6, respectively. The mole fraction of water is 0.7 for the presented data. The activity coefficients of 2-MPZ are found to be very less when compared to MDEA and H_2O (Figure 4a). The temperature dependency of the parameter is observed not to be high. Also, as a function of the MDEA concentration, the activity coefficients of 2-MPZ were found to show an inverse relationship. However, for both MDEA and H_2O , it does not change much. Insignificant deviations of H^E (excess enthalpy) and G^E (excess Gibbs free energy) with respect to the temperature change from 303.15 to 323.15 K are observed (Figure 4b). Nevertheless, both the properties were found to have negative values that increase as a function of the MDEA concentration. The

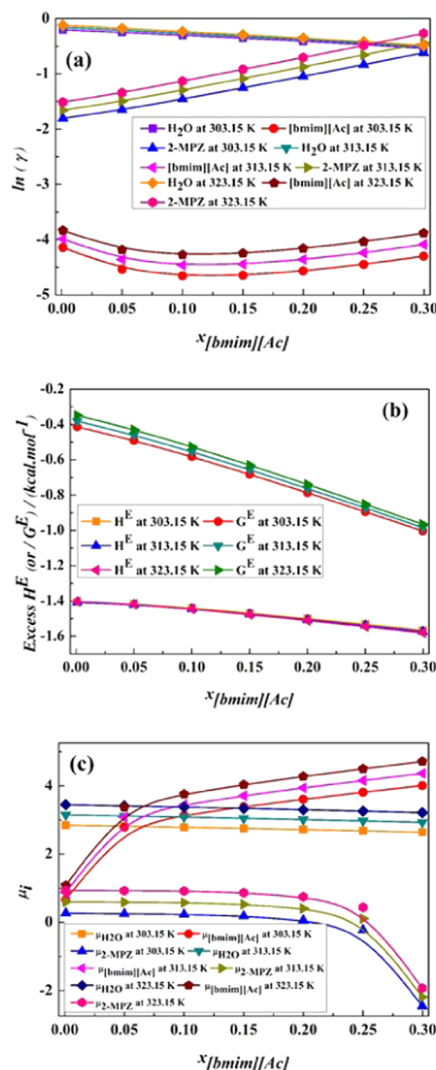


Figure 6. COSMO predicted (a) activity coefficient, (b) excess enthalpy and Gibb's free energy, and (c) chemical potential as a function of mole fraction of $[bmim][Ac]$ for the aq ($[bmim][Ac]$ + 2-MPZ) system at $x_{H_2O} = 0.7$.

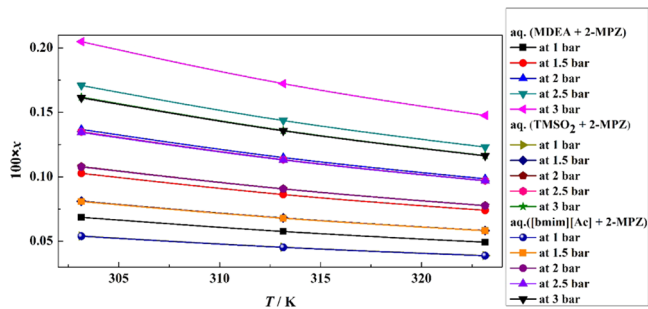


Figure 7. COSMO predicted CO₂ solubility of aq (3.509 m MDEA + 0.509 2-MPZ), aq (3.501 m TMSO₂ + 0.509 2-MPZ), and aq (3.507 m $[bmim][Ac]$ + 0.509 2-MPZ) as a function of temperature and pressure.

-ve G^E indicates the spontaneous mixing because of the thermodynamic driving forces between the involved components and -ve H^E indicates an exothermic reaction/mixing in both the systems that are proven by the values of heat of absorption.^{66,67} The chemical potential, on the other hand, is

observed to be more temperature-dependent. The values of μ_{H_2O} remain almost unchanged. Decreasing the concentration of 2-MPZ results in high chemical potential of MDEA and vice versa (Figure 4c).

Similarly, with respect to the TMSO₂ concentration, the activity coefficients of TMSO₂ and H₂O are observed to decrease and increase slightly simultaneously as a function of TMSO₂ (Figure 5a). The behavior of 2-MPZ is similar to that found for the aq (MDEA + 2-MPZ) system. The behavior of all three systems with respect to chemical potential is found to be very similar (Figures 5c and 6c). The activity coefficients for $[bmim][Ac]$ are very less when compared to 2-MPZ and H₂O at any given concentration (Figure 6a). This is also expected due to the lesser chemisorption but greater physisorption behavior conferred by the ionic liquid to the acid gas. Also, though the H^E and G^E values obtained in the aq ($[bmim][Ac]$ + 2-MPZ) system are negative but are a function of $[bmim][Ac]$, the values are found to further decrease unlike those for the other two systems (Figure 6b).

3.6. CO₂ Solubility in Aq (MDEA + 2-MPZ), Aq (TMSO₂ + 2-MPZ), and Aq ($[bmim][Ac]$ + 2-MPZ). The experimental measurement at the lab scale or estimation of CO₂ solubility in suitable solvents has been a key research area for application.^{29,34} Considering the lower partial pressures of CO₂ in the flue gas stream, the CO₂ solubility has been predicted using the activity coefficients estimated through COSMO-RS over the temperature and pressure range of 303.15–323.15 K and 1.0–3.0 bar for aq (MDEA + 2-MPZ), aq (TMSO₂ + 2-MPZ), and aq ($[bmim][Ac]$ + 2-MPZ) systems at varying compositions. The solubilities are presented in terms of the mole fraction of CO₂ in the liquid phase (x_{CO_2}). An inverse relationship between the CO₂ solubility and temperature for all of the studied solvent blends was observed (Figure 7). Further, although increasing the CO₂ pressure as well as the activator 2-MPZ concentration in all solvents resulted in an increase in CO₂ solubility (Table 11), however, in the case of the aq (MDEA + 2-MPZ) system, CO₂ solubility is observed to be almost similar over the chosen compositional range. This may be attributed to the fact that MDEA is a tertiary amine when compared with TMSO₂ and $[bmim][Ac]$, which have higher CO₂ solubility. Hence, with the increasing concentration of 2-MPZ in the aqueous blends of (MDEA + 2-MPZ), the concentration of MDEA is also simultaneously decreased. Hence, the CO₂ solubility at high MDEA concentration can be understood to be compensated by a decrease in the 2-MPZ concentration. Decisively, the highest CO₂ solubility is observed for the aq (MDEA + 2-MPZ) concentration at 303.15 K. However, it should be also considered that there may be a deviation when the same solvents are studied experimentally for CO₂ absorption. This discrepancy may be attributed to variables affecting the process, nonideality associated with gas and liquid phases, vapor pressures, temperature, maintenance of the partial pressure in the system, etc.

3.7. Estimation of Henry's Constant in CO₂ and N₂O and Free Energy of Solvation. Henry's constant signifies the physical solubility conferred by any solvent selectively to a gas that can either be measured experimentally or through the mathematical expressions available in the literature.⁶⁸ H_{CO_2} or H_{N_2O} is a contributive property through misfit in the intermolecular interactions, hydrogen bonding, and van der Waals forces of attraction. The estimation of Henry's law coefficient involves the estimation of solvation free energies, which are

Table 11. COSMO Predicted CO₂ Solubility ($100 \times x$) from 1.0 to 3.0 Bar Pressure in the Temperature Range of 303.15–323.15 K^a

(MDEA + 2-MPZ) (mol·kg ⁻¹)	P (bar)	T (K)			(TMSO ₂ + 2-MPZ) (mol·kg ⁻¹)	T (K)			([bmim][Ac] + 2-MPZ) (mol·kg ⁻¹)	T (K)		
		303.15	313.15	323.15		303.15	313.15	323.15		303.15	313.15	323.15
(3.509 + 0.509)	1.0	0.069	0.058	0.049	(3.501 + 0.509)	0.054	0.045	0.039	(3.507 + 0.509)	0.054	0.045	0.039
	1.5	0.103	0.086	0.074		0.081	0.068	0.058		0.081	0.068	0.058
	2.0	0.137	0.115	0.099		0.108	0.091	0.078		0.108	0.091	0.078
	2.5	0.171	0.144	0.123		0.135	0.113	0.097		0.135	0.113	0.097
	3.0	0.205	0.172	0.148		0.162	0.136	0.116		0.161	0.136	0.116
(3.017 + 1.008)	1.0	0.069	0.058	0.049	(3.012 + 1.008)	0.056	0.047	0.040	(3.002 + 1.008)	0.056	0.047	0.040
	1.5	0.103	0.087	0.074		0.084	0.071	0.061		0.084	0.070	0.060
	2.0	0.137	0.115	0.099		0.112	0.094	0.081		0.111	0.094	0.080
	2.5	0.171	0.144	0.123		0.141	0.118	0.101		0.139	0.117	0.100
	3.0	0.205	0.173	0.148		0.169	0.142	0.121		0.167	0.140	0.120
(2.502 + 1.509)	1.0	0.069	0.058	0.049	(2.500 + 1.509)	0.058	0.049	0.042	(2.510 + 1.509)	0.058	0.049	0.042
	1.5	0.103	0.086	0.074		0.088	0.074	0.063		0.087	0.073	0.063
	2.0	0.137	0.115	0.099		0.117	0.098	0.084		0.116	0.097	0.083
	2.5	0.171	0.144	0.123		0.146	0.122	0.105		0.144	0.121	0.104
	3.0	0.205	0.173	0.148		0.175	0.147	0.126		0.173	0.146	0.125

^ax is the mole fraction of CO₂ in the loaded solvent.

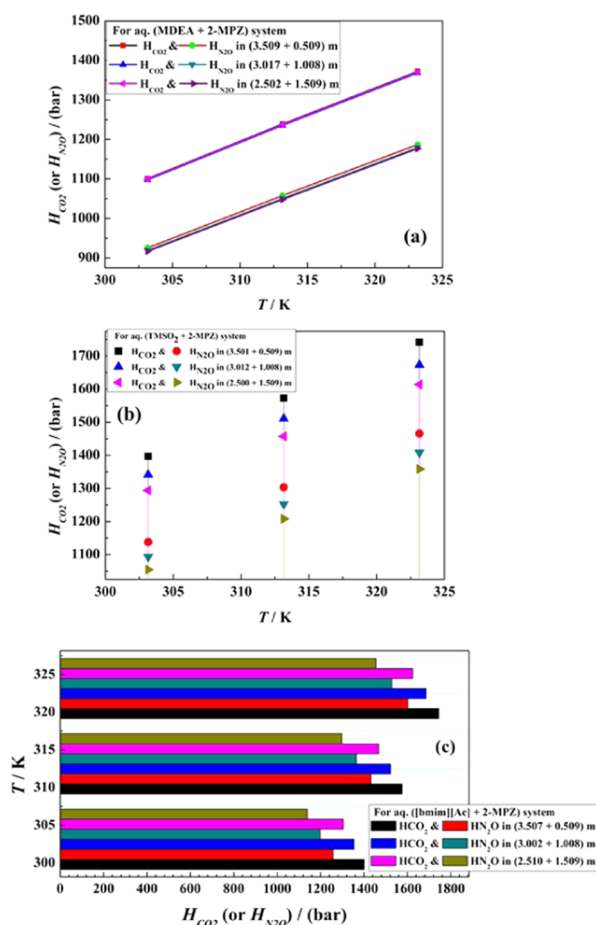


Figure 8. COSMO predicted Henry's constant of CO₂ and N₂O in (a) aq (MDEA + 2-MPZ), (b) aq (TMSO₂ + 2-MPZ), and (c) aq ([bmim][Ac] + 2-MPZ) systems as a function of composition and temperature.

further related to the chemical potential associated with the gas and solvent at a specified temperature and pressure (Table 2). The calculated results are reported in Figure 8 and Table 12 for all of the systems under study. A low value of Henry's law

coefficient indicates a higher CO₂ solubility. It can thus be inferred from the obtained results that increasing the concentration of 2-MPZ from ≈ 0.5 to ≈ 1.5 mol·kg⁻¹, for all base solvents of TMSO₂ and [bmim][Ac], yields an increase of physical solubility, whereas the maximum physical solubility in the case of aq (MDEA + 2-MPZ) is obtained at a 1.008 mol·kg⁻¹ concentration of 2-MPZ. Increasing the 2-MPZ concentration further in the aq (MDEA + 2-MPZ) system results in a decrease in physical solubility that may be owing to the fact that the number of amino groups in the overall blend has increased, which majorly contributes to chemical solubility. Further, the solubilities are found to be much higher at low temperatures for all systems. Henry's law coefficients for CO₂ and N₂O are obtained in the order: aq (MDEA + 2-MPZ) > aq (TMSO₂ + 2-MPZ) > aq ([bmim][Ac] + 2-MPZ) systems.

3.8. Estimation of the Dissociation Constant (pK_a) of MDEA and 2-MPZ. Proton exchange is considered to be one of the major reactions that occur during the interaction between CO₂ and amines.^{2,69} This proton exchange reaction rate constant is often described using the dissociation constant (pK_a) of the reaction. The $-\text{ve}$ log of pK_a of conjugate acid reveals the extent of basicity offered by the chosen solvent. The above property can be either measured experimentally using the acid–base titration method or can also be predicted using quantum methods. The dissociation constants of 2-MPZ and MDEA have been calculated using COSMO. Initially, single conformers with ground-state energy were selected. The selected geometry was then edited to create a cationic structure of the same. Further, this cationic structure was optimized to calculate the energy using Turbomole software. The generated cationic structures along with the optimized energy are presented in Figure 9. Based on the free-energy change in any molecule and corresponding cationic structure, the pK_a values were estimated in water, acetonitrile, and tetrahydrofuran solvents. The predicted pK_a values of MDEA and 2-MPZ are given in Table 13 at 25 °C. Simulated results show that the pK_a values of 2-MPZ are relatively higher compared with MDEA in all solvents, demonstrating it to have the possibility of enhanced CO₂ solubility.

Table 12. COSMO Predicted Henry's Constant (H , bar) and Gibbs' Free Energy of Solvation (ΔG_s , kcal·mol $^{-1}$) in the Temperature Range of 303.15–323.15 K^a

	H	T (K)			T (K)			T (K)					
		aq (MDEA + 2-MPZ) (mol·kg $^{-1}$)	303.15	313.15	323.15	aq (TMSO ₂ + 2-MPZ) (mol·kg $^{-1}$)	303.15	313.15	323.15	aq ([bmim] [Ac] + 2-MPZ) (mol·kg $^{-1}$)	303.15	313.15	323.15
CO ₂	H	(3.509 + 0.509)	1100.644	1238.922	1371.935	(3.501 + 0.509)	1396.815	1572.858	1741.921	(3.507 + 0.509)	1400.345	1575.528	1744.370
	ΔG_s		4.219	4.432	4.639		4.363	4.580	4.792		4.364	4.582	4.793
N ₂ O	H		925.420	1057.576	1186.703		1137.946	1303.575	1465.748		1257.580	1432.083	1602.166
	ΔG_s		4.115	4.333	4.546		4.239	4.464	4.681		4.299	4.522	4.739
CO ₂	H	(3.017 + 1.008)	1097.466	1235.339	1368.044	(3.012 + 1.008)	1341.653	1510.724	1673.258	(3.002 + 1.008)	1353.436	1522.609	1685.678
	ΔG_s		4.217	4.430	4.637		4.338	4.555	4.766		4.344	4.560	4.771
N ₂ O	H		918.970	1050.473	1179.077		1093.273	1252.391	1408.311		1197.891	1365.014	1528.088
	ΔG_s		4.110	4.329	4.542		4.215	4.439	4.656		4.270	4.492	4.708
CO ₂	H	(2.502 + 1.509)	1099.129	1237.204	1370.175	(2.500 + 1.509)	1293.996	1457.038	1613.922	(2.510 + 1.509)	1304.265	1467.245	1624.386
	ΔG_s		4.218	4.431	4.638		4.317	4.533	4.743		4.321	4.537	4.747
N ₂ O	H		916.253	1047.660	1176.281		1054.550	1208.024	1358.521		1138.477	1298.193	1454.226
	ΔG_s		4.109	4.328	4.540		4.193	4.416	4.633		4.240	4.461	4.676

^a1 bar of gas per 1 mol of solvent is taken as the reference state for the H and ΔG calculation.

4. CONCLUSIONS

A comprehensive thermodynamic analysis through the COSMO-RS theory has been carried out for the proposed enhanced CO₂ solubility by 2-methylpiperazine in aqueous solvents of *N*-methylidiethanolamine, sulfolane, and 1-butyl-2-methylimidazolium acetate. The appropriateness of chosen solvents, i.e., MDEA, TMSO₂, and [bmim][Ac], and their blends with 2-MPZ is determined using σ potential and σ surface analyses. The results indicate the suitability of 2-MPZ for a variety of solvents under study. Conclusively, the aqueous blend of MDEA and 2-MPZ is preferred over other solvents. Vapor pressures of the solvents, pure component density, and viscosity are also simulated and compared with experimental data, indicating a featured calculation through the involved method. The minimum deviations for estimation of vapor pressure and density for [bmim][Ac] with % AAD are 13.407 and 1.067, respectively. Additionally, activity coefficient-based thermodynamic models, viz., NRTL, WILSON, and UNIQUAC 4 model parameters, are assessed for aq (MDEA + 2-MPZ), aq (TMSO₂ + 2-MPZ), and aq ([bmim][Ac] + 2-MPZ) systems. The nonideal behavior of the systems is indicated by the simulated values of infinite dilution activity coefficients, activity coefficient, excess enthalpy, excess Gibbs' free energy, and chemical potential. CO₂ solubility in all of the solvents is predicted at 303.15–323.15 K and 1.0–3.0 bar pressure. Moreover, COSMO anticipated pK_a values of MDEA and 2-MPZ indicate a higher pK_a value for 2-MPZ than MDEA. This further confirms the expected higher CO₂ solubility in 2-MPZ when compared with MDEA.

■ AUTHOR INFORMATION

Corresponding Author

Ramesh Singh – Department of Chemical Engineering, University of Pittsburgh at Johnstown, Johnstown, Pennsylvania 15904, United States; orcid.org/0000-0002-0738-3345; Phone: +1-814-269-7269; Email: rsingh@pitt.edu

Author

Sweta Balchandani – Department of Chemical Engineering, Indian Institute of Technology Guwahati, Guwahati 781039, India; CO₂ Research Group, Department of Chemical

Engineering School of Technology, Pandit Deendayal Petroleum University, Gandhinagar 382007, India

Complete contact information is available at:

<https://pubs.acs.org/10.1021/acsomega.0c05298>

Notes

The authors declare no competing financial interest.

■ ACKNOWLEDGMENTS

The authors thank Pandit Deendayal Petroleum University, Gandhinagar, India, for providing the necessary computational and experimentation facilities.

■ REFERENCES

- Shirazizadeh, H. A.; Haghtalab, A. Measurement and modeling of CO₂ solubility in binary aqueous DMSO and MDEA and their ternary mixtures at different temperatures and compositions. *Fluid Phase Equilib.* **2020**, No. 112845.
- Afkhamipour, M.; Mofarahi, M.; Rezaei, A.; Mahmoodi, R.; Lee, C. H. Experimental and theoretical investigation of equilibrium absorption performance of CO₂ using a mixed 1-dimethylamino-2-propanol (1DMA2P) and monoethanolamine (MEA) solution. *Fuel* **2019**, 256, No. 115877.
- Zong, L.; Chen, C. C. Thermodynamic modeling of CO₂ and H₂S solubilities in aqueous DIPA solution, aqueous sulfolane-DIPA solution, and aqueous sulfolane-MDEA solution with electrolyte NRTL model. *Fluid Phase Equilib.* **2011**, 306, 190–203.
- Chen, X.; Rochelle, G. T. Modeling of CO₂ absorption kinetics in aqueous 2-methylpiperazine. *Ind. Eng. Chem. Res.* **2013**, 52, 4239–4248.
- Khan, S. N.; Hailegiorgis, S. M.; Man, Z.; Shariff, A. M.; Garg, S. Thermophysical properties of aqueous 1-butyl-3-methylimidazolium acetate [bmim][Ac] + monoethanolamine (MEA) hybrid as a solvent for CO₂ capture. *Procedia Eng.* **2016**, 148, 1326–1331.
- Taboada, M. E.; Vélez, D. M.; Galleguillos, H. R.; Gruber, T. A. Solubility, density, viscosity, electrical conductivity, and refractive index of saturated solutions of lithium hydroxide in water + ethanol. *J. Chem. Eng. Data* **2005**, 50, 187–190.
- Sanku, M. G.; Svensson, H. Modelling the precipitating non-aqueous CO₂ capture system AMP-NMP, using the unsymmetric electrolyte NRTL. *Int. J. Greenhouse Gas Control* **2019**, 89, 20–32.
- Mota Martinez, M. T.; Kroon, M. C.; Peters, C. J. Modeling CO₂ solubility in an ionic liquid: a comparison between a cubic and a group contribution EoS. *J. Supercrit. Fluids* **2015**, 101, 54–62.

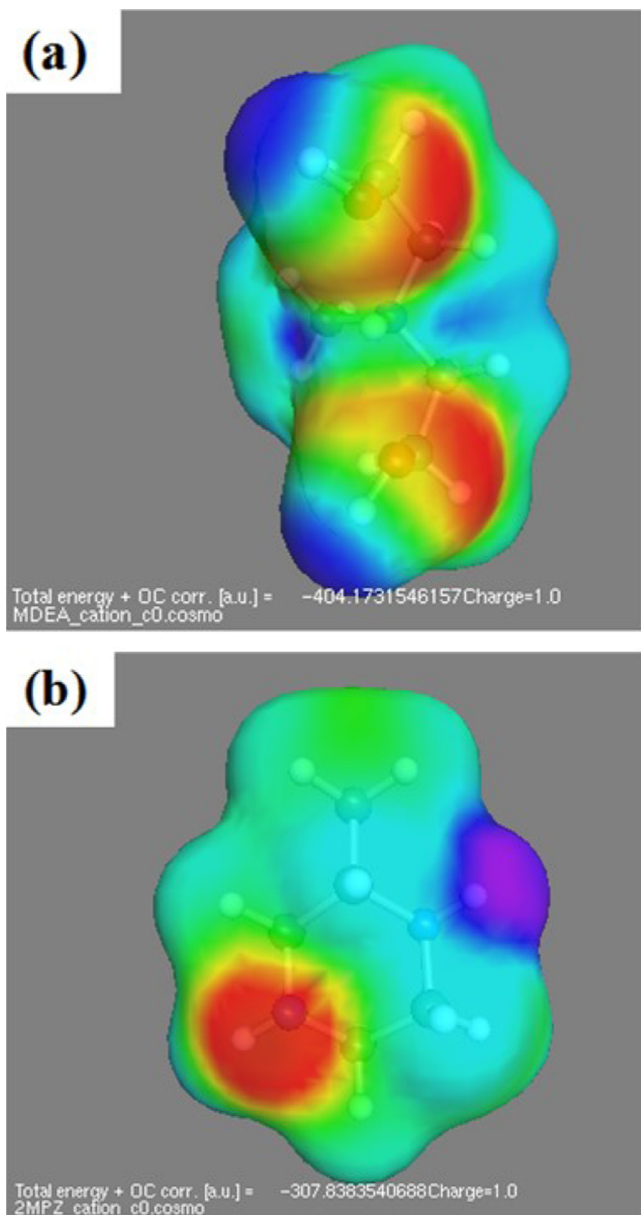


Figure 9. Turbomole optimized generated (a) *N*-methyldiethanolamine cation and (b) 2-methylpiperazine cation.

Table 13. pK_a Values of MDEA and 2-MPZ at 298.15 K in Various Solvents

	solvent	H ₂ O	acetonitrile	tetrahydrofuran
pK _a	MDEA	3.758	12.176	8.836
	2-MPZ	5.885	14.333	10.387

(9) Liu, S.; Ling, H.; Gao, H.; Tontiwachwuthikul, P.; Liang, Z.; Zhang, H. Kinetics and new bronsted correlations study of CO₂ absorption into primary and secondary alkalamines with and without steric-hindrance. *Sep. Purif. Technol.* **2020**, 233, No. 115998.

(10) Papadopoulos, A. I.; Shavlieva, G.; Papadokonstantakis, S.; Seferlis, P.; Perdomo, F. A.; Galindo, A.; Jackson, G.; Adjiman, C. S. An approach for simultaneous computer-aided molecular design with holistic sustainability assessment: application to phase-change CO₂ capture solvents. *Comput. Chem. Eng.* **2020**, 135, No. 106769.

(11) Gonzalez-Miquel, M.; Talreja, M.; Ethier, A. L.; Flack, K.; Switzer, J. R.; Biddinger, E. J.; Pollet, P.; Palomar, J.; Rodriguez, F.; Eckert, C. A.; Liotta, C. L. COSMO-RS studies: structure-property

relationships for CO₂ capture by reversible ionic liquids. *Ind. Eng. Chem. Res.* **2012**, 51, 16066–16073.

(12) Kim, I.; Hoff, K. A.; Hessen, E. T.; Warberg, T. H.; Svendsen, H. F. Enthalpy of absorption of CO₂ with alkanolamine solutions predicted from reaction equilibrium constants. *Chem. Eng. Sci.* **2009**, 64, 2027–2038.

(13) Dehghani, M.; Asghari, M.; Mohammadi, A. H.; Mokhtari, M. Molecular simulation and Monte Carlo study of structural-transport-properties of PEBA-MFI zeolite mixed matrix membranes for CO₂, CH₄ and N₂ separation. *Comput. Chem. Eng.* **2017**, 103, 12–22.

(14) Jayarathna, S. A.; Lie, B.; Melaaen, M. C. Dynamic modelling of the absorber of a post-combustion CO₂ capture plant: modeling and simulations. *Comput. Chem. Eng.* **2013**, 53, 178–189.

(15) Haron, N.; Sairi, N. A.; Lee, V. S. Microstructures, interactions and dynamics properties studies of *N*-methyldiethanolamine + guanidinium triflate ionic liquid + water tertiary system at the standard temperature. *Mol. Simul.* **2016**, 42, 655–666.

(16) Mohan, O.; Trinh, Q. T.; Banerjee, A.; Mushrif, S. H. Predicting CO₂ adsorption and reactivity on transition metal surfaces using popular density functional theory methods. *Mol. Simul.* **2019**, 45, 1163–1172.

(17) Houndoungbo, Y.; Kuczera, K.; Subramaniam, B.; Laird, B. B. Prediction of phase equilibria and transport properties in carbon-dioxide expanded solvents by molecular simulation. *Mol. Simul.* **2007**, 33, 861–869.

(18) Whangbo, M.-H.; Gordon, E. E.; Xiang, H.; Koo, H. J.; Lee, C. Prediction of spin orientations in terms of HOMO-LUMO interactions using spin-orbit coupling as perturbation. *Acc. Chem. Res.* **2015**, 48, 3080–3087.

(19) Klamt, A. COSMO-RS for aqueous solvation and interfaces. *Fluid Phase Equilib.* **2016**, 407, 152–158.

(20) Ossman, T.; Fabre, G.; Trouillas, P. Interaction of wine anthocyanin derivatives with lipid bilayer membranes. *Comput. Theor. Chem.* **2016**, 1077, 80–86.

(21) Mehling, T.; Ingram, T.; Storm, S.; Bobe, U.; Liu, F.; Michel, M.; Smirnova, I. Estimation of LPC/water partition coefficients using molecular modeling and micellar liquid chromatography. *Colloids Surf., A* **2013**, 431, 105–113.

(22) Ritter, E.; Racheva, R.; Jakobtorweihen, S.; Smirnova, I. Influence of D-glucose as additive on thermodynamics and physical properties of aqueous surfactants two-phase systems for the continuous micellar extraction. *Chem. Eng. Res. Des.* **2017**, 121, 149–162.

(23) Dolzonek, J.; Cho, C. W.; Stepnowski, O.; Markiewicz, M.; Thoming, J.; Stolte, S. Membrane partitioning of ionic liquid cations, anions and ion pairs- estimating the bioconcentration potential of organic ions. *Environ. Pollut.* **2017**, 228, 378–389.

(24) Yordanova, D.; Smirnova, I.; Jakobtorweihen, S. Molecular modeling of Triton X Micelles: force field parameters self-assembly, and partition equilibria. *J. Chem. Theory Comput.* **2015**, 11, 2329–2340.

(25) Storm, S.; Aschenbrenner, D.; Smirnova, I. Reverse miscellar extraction of amino acids and complex enzyme mixtures. *Sep. Purif. Technol.* **2014**, 123, 23–24.

(26) Turchi, M.; Cai, Q.; Lian, G. An evaluation of in-silico methods for predicting solute partition in multiphase complex fluids- a case study of octanol/water partition coefficient. *Chem. Eng. Sci.* **2019**, 197, 150–158.

(27) Liang, X.; Li, Y.; Wu, X.; Shen, J.; Lee, K. Y. Nonlinearity analysis and multi-model modeling of an MEA-based post-combustion CO₂ capture process for advanced control design. *Appl. Sci.* **2018**, 8, No. 1053.

(28) Karlsson, H.; Svensson, H. Rate of absorption for CO₂ absorption systems using a wetted wall column. *Energy Procedia* **2017**, 114, 2009–2023.

(29) Kim, Y. E.; Choi, J. H.; Nam, S. C.; Yoon, Y. I. CO₂ absorption capacity using aqueous potassium carbonate with 2-methylpiperazine and piperazine. *J. Ind. Eng. Chem.* **2012**, 18, 105–110.

- (30) Yuan, Y.; Sherman, B.; Rochelle, G. T. Effects of viscosity on CO₂ absorption in aqueous piperazine / 2-methylpiperazine. *Energy Procedia* **2017**, *114*, 2103–2120.
- (31) Hafizi, A.; Mokari, M. H.; Khalifeh, R.; Farsi, M.; Rahimpour, M. R. Improving the CO₂ solubility in aqueous mixture of MDEA and different polyamine promoters: The effects of primary and secondary functional groups. *J. Mol. Liq.* **2019**, No. 111803.
- (32) Zong, L.; Chen, C. C. Thermodynamic modeling of CO₂ and H₂S solubilities in aqueous DIPA solution, aqueous sulfolane-DIPA solution, and aqueous sulfolane-MDEA solution with electrolyte NRTL model. *Fluid Phase Equilib.* **2011**, *306*, 190–203.
- (33) Shokouhi, M.; Jalili, A. H.; Zoghi, A. T.; Ahari, J. S. Carbon dioxide solubility in aqueous sulfolane solution. *J. Chem. Thermodyn.* **2019**, *132*, 62–72.
- (34) Jalili, A. H.; Shokouhi, M.; Samani, F.; Jenab, M. J. Measuring the solubility of CO₂ and H₂S in sulfolane and the density and viscosity of saturated liquid binary mixtures of (sulfolane + CO₂) and (sulfolane + H₂S). *J. Chem. Thermodyn.* **2015**, *85*, 13–25.
- (35) Safarov, J.; Geppert-Rybczynska, M.; Kul, I.; Hassel, E. Thermophysical properties of 1-butyl-3-methylimidazolium acetate over a wide range of temperatures and pressures. *Fluid Phase Equilib.* **2014**, *383*, 144–155.
- (36) Osman, K.; Ramjugernath, D.; Coquelet, C. CO₂ solubility in hybrid solvents containing 1-butyl-3-methylimidazolium tetrafluoroborate and mixtures of alkanolamine. *J. Chem. Eng. Data* **2015**, *60*, 2380–2391.
- (37) Chakravarty, T.; Phukan, U.; Weilund, R. Reaction of acid gases with mixtures of amines. *Chem. Eng. Prog.* **1985**, *81*, 32–36.
- (38) Kohl, A. L.; Nielsen, R. *Gas Purification*; Gulf Professional Publishing, 1997.
- (39) Aghehrochaboki, R.; Chaboki, Y. A.; Maleknia, S. A.; Irani, V. Polyethyleneimine functionalized graphene oxide/methyldiethanolamine nanofluid: preparation, characterization, and investigation of CO₂ absorption. *J. Environ. Chem. Eng.* **2019**, *7*, No. 103285.
- (40) Eckert, F.; Klamt, A. COSMOtherm, release 19.0.1; COSMOlogic GmbH & Co. KG: Leverkusen, 2013.
- (41) Sumon, K. Z.; Henni, A. Ionic liquids for CO₂ capture using COSMO-RS: effect of structure, properties and molecular interactions on solubility and selectivity. *Fluid Phase Equilib.* **2011**, *310*, 39–55.
- (42) Klamt, A.; Eckert, F. COSMO-RS: a novel and efficient method for the priori prediction of thermophysical data of liquids. *Fluid Phase Equilib.* **2000**, *172*, 43–72.
- (43) Matheswaran, P.; Wilfred, C. D.; Kurnia, K. A.; Ramli, A. Overview of activity coefficient of thiophene at infinite dilution in ionic liquids and their modeling using COSMO-RS. *Ind. Eng. Chem. Res.* **2016**, *55*, 788–797.
- (44) Sun, C.; Dutta, P. K. Infrared Spectroscopic Study of Reaction of Carbon Dioxide with Aqueous Monoethanolamine Solutions. *Ind. Eng. Chem. Res.* **2016**, *55*, 6276–6283.
- (45) Richner, G.; Puxty, G. Assessing the Chemical Speciation during CO₂ absorption by Aqueous Amines using in Situ FTIR. *Ind. Eng. Chem. Res.* **2012**, *51*, 14317–14324.
- (46) Valderrama, J. O.; Forero, L. A. An analytical expression for the vapor pressure of ionic liquids based on an equation of state. *Fluid Phase Equilib.* **2012**, *317*, 77–83.
- (47) Peng, D. Y.; Robinson, D. B. A New Two-Constant Equation of State. *Ind. Eng. Chem. Fundam.* **1976**, *15*, 59–64.
- (48) Katritzky, A. R.; Slavov, S. H.; Dobchev, D. A.; Karelson, M. Rapid QSPR model development technique for prediction of vapor pressure of organic compounds. *Comput. Chem. Eng.* **2007**, *31*, 1123–1130.
- (49) Lei, Z.; Yu, G.; Su, Y.; Dai, C. Vapor pressure measurements and predictions for the binary and ternary systems containing ionic liquid [EMIM] [Tf₂N]. *J. Mol. Liq.* **2017**, *231*, 272–280.
- (50) Hekayati, J.; Roosta, A.; Javanmardi, J. On the prediction of the vapor pressure of ionic liquids based on the principle of corresponding states. *J. Mol. Liq.* **2017**, *225*, 118–126.
- (51) Balchandani, S.; Mandal, B. P.; Dharaskar, S. Measurements and modeling of vapor liquid equilibrium of CO₂ in amine activated imidazolium ionic liquid solvents. *Fluid Phase Equilib.* **2020**, *521*, No. 112643.
- (52) Joshipura, M. H.; Dabke, S. P.; Subrahmanyam, N. Development and comparison of cohesion function relationship for PR equation of state. *Int. J. Chem. Eng. Res.* **2009**, *1*, 123–134.
- (53) Valderrama, J. O.; Forero, L. A. An analytical expression for the vapor pressure of ionic liquids based on an equation of state. *Fluid Phase Equilib.* **2012**, *317*, 77–83.
- (54) Kumar, S.; Cho, J. H.; Moon, I. Ionic liquid-amine blends and CO₂ BOLs: prospective solvents for natural gas sweetening and CO₂ capture technology-a review. *Int. J. Greenhouse Gas Control* **2014**, *20*, 87–116.
- (55) Wappel, D.; Gronald, G.; Kalb, R.; Draxler, J. Ionic liquids for post-combustion CO₂ absorption. *Int. J. Greenhouse Gas Control* **2010**, *4*, 486–494.
- (56) Paul, S.; Ghoshal, A. K.; Mandal, B. P. Kinetics of absorption of carbon dioxide into aqueous blends of 2-(1-piperazinyl)-ethylamine and N-methyldiethanolamine. *Chem. Eng. Sci.* **2009**, *64*, 1618–1622.
- (57) Balchandani, S.; Mandal, B. P.; Dharaskar, S.; Kumar, A.; Bandyopadhyay, S. S. Thermally induced characterization and modeling of physiochemical, acoustic rheological, and thermodynamic properties of novel blends of (HEF + AEP) and (HEF + AMP) for CO₂/H₂S absorption. *Environ. Sci. Pollut. Res.* **2019**, *26*, 32209–32223.
- (58) Aspen Technology Inc. *Aspen Physical Property System*, version 7.1; Aspen Technology Inc.: Cambridge, 2008.
- (59) Bara, J. E.; Moon, J. D.; Reclusado, K. R.; Whitley, J. W. COSMOtherm as a tool for estimating the thermophysical properties of alkylimidazoles as solvents for CO₂ separations. *Ind. Eng. Chem. Res.* **2013**, *52*, 5498–5506.
- (60) Diedenhofen, M.; Eckert, F.; Klamt, A. Prediction of infinite dilution activity coefficients of organic compounds in ionic liquids using COSMO-RS. *J. Chem. Eng. Data* **2003**, *48*, 475–479.
- (61) Putnam, R.; Taylor, R.; Klamt, A.; Eckert, F.; Schiller, M. Prediction of infinite dilution activity coefficients using COSMO-RS. *Ind. Eng. Chem. Res.* **2003**, *42*, 3635–3641.
- (62) Paduszyński, K. An overview of performance of COSMO-RS approach in predicting activity coefficients of molecular solutes in ionic liquids and derived properties at infinite dilution. *Phys. Chem. Chem. Phys.* **2017**, *19*, 11835–11850.
- (63) Voutsas, E. C.; Tassios, D. P. Prediction of Infinite-Dilution Activity Coefficients in Binary Mixtures with UNIFAC. A Critical Evaluation. *Ind. Eng. Chem. Res.* **1996**, *35*, 1438–1445.
- (64) Dash, S. K.; Samanta, A. N.; Bandyopadhyay, S. S. Solubility of carbon dioxide in aqueous solution of 2-amino-2-methyl-1-propanol and piperazine. *Fluid Phase Equilib.* **2011**, *307*, 166–174.
- (65) Renon, H.; Prausnitz, J. M. Local compositions in thermodynamic excess functions for liquid mixtures. *AIChE J.* **1968**, *14*, 135–144.
- (66) Liang, Y.; Liu, H.; Rongwong, W.; Liang, Z.; Idem, R.; Tontowachwuthikul, P. Solubility, absorption heat and mass transfer studies of CO₂ absorption into aqueous solution of 1-dimethylamino-2-propanol. *Fuel* **2015**, *144*, 121–129.
- (67) Ling, H.; Liu, S.; Gao, H.; Zhang, H.; Liang, Z. Solubility of N₂O, equilibrium solubility, mass transfer study and modeling of CO₂ absorption into aqueous monoethanolamine (MEA)/1-dimethylamino-2-propanol (1DMA2P) solution for post-combustion CO₂ capture. *Sep. Purif. Technol.* **2020**, *232*, No. 115957.
- (68) Edwards, T. J.; Maurer, G.; Newman, J.; Prausnitz, J. M. Vapor-liquid equilibria in multicomponent aqueous solutions of volatile weak electrolytes. *AIChE J.* **1978**, *24*, 966–976.
- (69) Benamor, A.; Aroua, M. K. Modeling of CO₂ solubility and carbamate concentration in DEA, MDEA and their mixtures using Deshmukh-Mather model. *Fluid Phase Equilib.* **2005**, *231*, 150–162.